AFRL-OSR-VA-TR-2013-0568

INVESTIGATION OF HIGHLY UNSTEADY AERODYNAMICS OF FLAPPING WINGS WITH/WITHOUT A FLEXIBLE TRAILING EDGE USING HIGH RESOLUTION MTV MEASUREMENTS

MANOOCHEHR KOOCHESFAHANI

MICHIGAN STATE UNIVERSITY

10/15/2013
Final Report

AIR FORCE RESEARCH LABORATORY
AF OFFICE OF SCIENTIFIC RESEARCH (AFOSR)/RSA
ARLINGTON, VIRGINIA 22203
AIR FORCE MATERIEL COMMAND

REPORT DOCUMENTATION PAGE

Form Approved
OMB No. 0704-0188

1. REPORT DATE *(DD-MM-YYYY)*	**2. REPORT TYPE**	**3. DATES COVERED** *(From - To)*
14-10-2013	Final Report	15 July 2010 - 14 July 2013

4. TITLE AND SUBTITLE

Investigation of Highly Unsteady Aerodynamics of Flapping Wings With/Without a Flexible Training Edge Using High Resolution MTV Measurements

5a. CONTRACT NUMBER

5b. GRANT NUMBER
FA9550-10-1-0342

5c. PROGRAM ELEMENT NUMBER

6. AUTHOR(S)
Ahmed M. Naguib
Manoochehr M. Koochesfahani

5d. PROJECT NUMBER

5e. TASK NUMBER

5f. WORK UNIT NUMBER

7. PERFORMING ORGANIZATION NAME(S) AND ADDRESS(ES)
Michigan State University
Contracts & Grants Administration
301 Administration Building
East Lansing, MI 48824-1046

8. PERFORMING ORGANIZATION REPORT NUMBER

9. SPONSORING / MONITORING AGENCY NAME(S) AND ADDRESS(ES)
USAF, AFRL DUNS 143574726
AF Office of Scientific Research
875 N. Randolph St. Room 3112
Arlington, VA 22203

10. SPONSOR/MONITOR'S ACRONYM(S)
AFOSR

11. SPONSOR/MONITOR'S REPORT NUMBER(S)

12. DISTRIBUTION / AVAILABILITY STATEMENT
Distribution A - Approved For Public Release

13. SUPPLEMENTARY NOTES

14. ABSTRACT

A three-year coordinated experimental and computational investigation is carried out to study the fundamental aerodynamics of oscillating airfoils in the chord Reynolds number range of 2,000 - 60,000. The objective of the investigation is to establish the connection between the airfoil motion trajectory, the trailing edge flexure, the time history of vorticity flux at the trailing edge, the pattern of shed vorticity and its evolution, and the conditions for generation of thrust/drag and lift. The results show that the non-dimensional spacing and circulation of the wake vortices as well as the mean thrust coefficient acting on the airfoil are similar for both rigid and flexible airfoils at the same Strouhal number, if the latter is computed using the actual airfoil's trailing edge oscillation amplitude. Furthermore, it is discovered that the Reynolds number has a significant influence on the reduced frequency and Strouhal number at which the wake vortex arrangement switches to the "reversed" von Karman street configuration and the mean streamwise force changes from drag to thrust. This study has also resulted in the development of new measurement techniques that will make possible in the future measurements of the pressure and shear stress distribution on flexible and moving surfaces.

15. SUBJECT TERMS

16. SECURITY CLASSIFICATION OF:			**17. LIMITATION OF ABSTRACT**	**18. NUMBER OF PAGES**	**19a. NAME OF RESPONSIBLE PERSON**
a. REPORT	**b. ABSTRACT**	**c. THIS PAGE**	SAR		Manoochehr Koochesfahani
U	U	U			**19b. TELEPHONE NUMBER** *(include area code)* (517) 353 5311

Standard Form 298 (Rev. 8-98)
Prescribed by ANSI Std. Z39.18

I. Background

This investigation is motivated by developing physical understanding of fundamental aspects of the aerodynamics of Unmanned Micro Air Vehicles (UMAVs). For a typical UMAV (Wilson, 1998), the small size of the device (wing chord of order 2 cm) and relatively slow flying speed (of order 10 m/s) result in a wing chord Reynolds number Re_c of order 10^4. Understanding of the aerodynamics at this low range of Reynolds numbers is lacking as traditional aerodynamics knowledge is based on high Reynolds number airfoils with thin attached boundary layers that operate under steady or quasi-steady conditions. Faced by the challenges of adequate lift generation in low Reynolds number flight based on traditional aerodynamics, and observation of nature's flying animals, a major departure in UMAV aerodynamics is the considerations of flapping wing designs where highly unsteady operating conditions are to be exploited instead of avoided (Lai and Platzer, 1999, Young and Lai, 2004, and Anderson *et al.*, 1998) . Added to this are the additional complexities introduced by highly 3-D low-aspect ratio wings that might also include surface flexibility, along with high-amplitude complicated motion trajectories, and gust response/tolerance. The problem is, indeed, multi-dimensional and immensely challenging.

The behavior of flow around airfoils executing highly unsteady motions has of course been studied for decades. The classical unsteady aerodynamic theory of oscillating airfoils (Theodorsen, 1935, and von Kármán and Sears, 1938) was developed as a result of interest in aircraft flutter problems. This theory later found extensive use in bio-fluid-dynamics, and the propulsion of certain species of birds, insects, and aquatic animals (Lighthill, 1975, and Wu, 1971). The main elements of the classical analysis are the potential flow along with linearized boundary conditions, small perturbation velocities, and the assumption of a planar vortex wake. All of these assumptions, appropriate for thin airfoils under small amplitude unsteady motions along with thin boundary layers over the airfoil, fail for the low Reynolds number unsteady airfoils of UMAVs. Even though nonlinear processes such as rolled-up wake vorticity have been addressed using numerical techniques (Giesing, 1968, Djojodihardjo and Widnall, 1969, and Vezza and Galbraith, 1985), all of these approaches still rely on potential flow theory and vortex methods where the strength of the vorticity shed into the wake is determined from the application of the Kutta condition at the trailing edge. In low Reynolds number airfoils where the boundary layer thickness at the trailing edge can be significantly larger than the trailing edge thickness, and under highly unsteady conditions, the conditions that should be imposed at the trailing edge become less clear than the Kutta condition used in inviscid analysis (Koochesfahani and Bohl, 2002).

Relevant to current UMAV efforts is also the large body of knowledge that is available from previous studies connected to dynamic stall (McCroskey, 1982) and significant developments in computational capabilities for such high amplitude unsteady airfoil motions, in particular those at AFRL which are of interest to this proposal (Visbal, 1986, and Visbal and Shang, 1989). Nevertheless, recent studies in UMAV aerodynamics have lead to the conclusion that the current state of knowledge, predictive capabilities, and experimental data are insufficient regarding the fundamental unsteady aerodynamics of low Reynolds number UMAVs (Shyy *et al.*, 2008) . The coordinated experimental and computational efforts undertaken in the present investigation is aimed at improving our fundamental understanding of low Reynolds number unsteady aerodynamics and, in conjunction with other AFOSR supported efforts and AFRL, contributing to improved predictive capabilities.

II. Objectives

The specific focus of the present project is the unsteady aerodynamics of oscillating airfoils with/without a flexible trailing edge in the chord Reynolds number range of $2\times10^3 - 6\times10^4$. The study encompasses various airfoil motion trajectories (pure pitch, pure plunge, combined pitch-plunge, asymmetric trajectory, etc.), and a range of oscillation frequencies and amplitudes. For such airfoils, we seek to establish the connection between the airfoil motion trajectory, the trailing edge flexure, the time history of vorticity flux at the trailing edge, the pattern of shed vorticity and its evolution, and the conditions for generation of thrust/drag and lift. In addition, we examine how these processes are influenced by aeroelastic parameters of the trailing edge and aspect ratio. The investigation is carried out using coordinated experiments and computations.

III. Methods

IV.1. Three-Degree of Freedom (3 DOF) System and Water Tunnel Modification

The proposed work required significant infrastructure modification of the 61 cm × 61 cm water tunnel test facility at the Turbulent Mixing and Unsteady Aerodynamics Laboratory (TMUAL) at MSU. This modification, which was completed successfully, included two parts: (I) the addition of two large quartz inserts (45.7 cm-high × 89 cm-wide × 12.7 cm-deep) into one of the acrylic side walls of the 61 cm × 61 cm × 243 cm test section (to allow UV laser light to pass through for MTV measurements); (II) the acquisition, assembly, mounting and operation verification of a three degree of freedom (3 DOF) rig to allow pitch, heave, and perch maneuvers of rigid and flexible airfoils. Details concerning these modifications may be found in Figures 1 and 2 and associated captions.

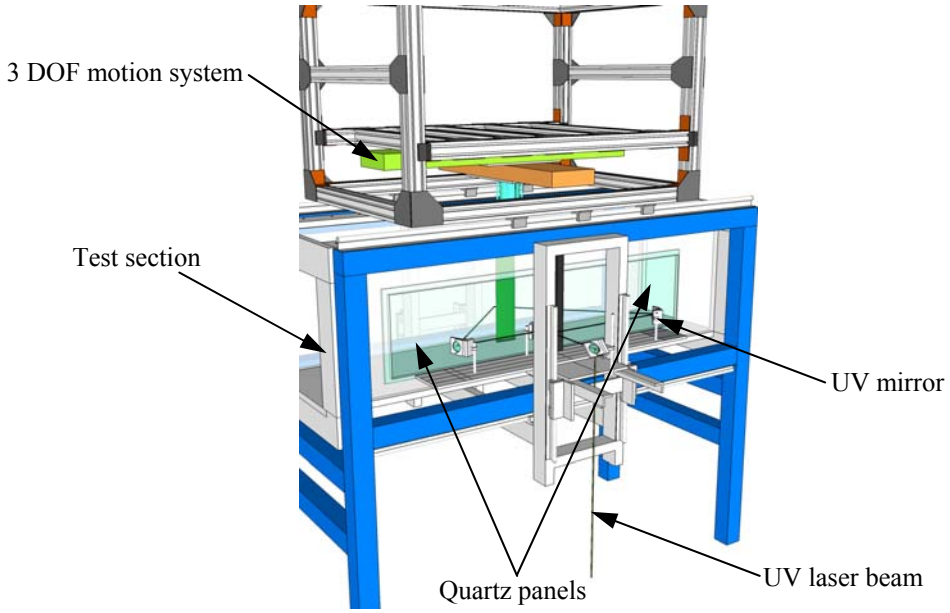

Figure 1. Water tunnel test-section cut-out showing the new quartz inserts and the 3 DOF motion system. The sketch also depicts a typical UV laser beam path for Molecular Tagging Velocimetry measurements

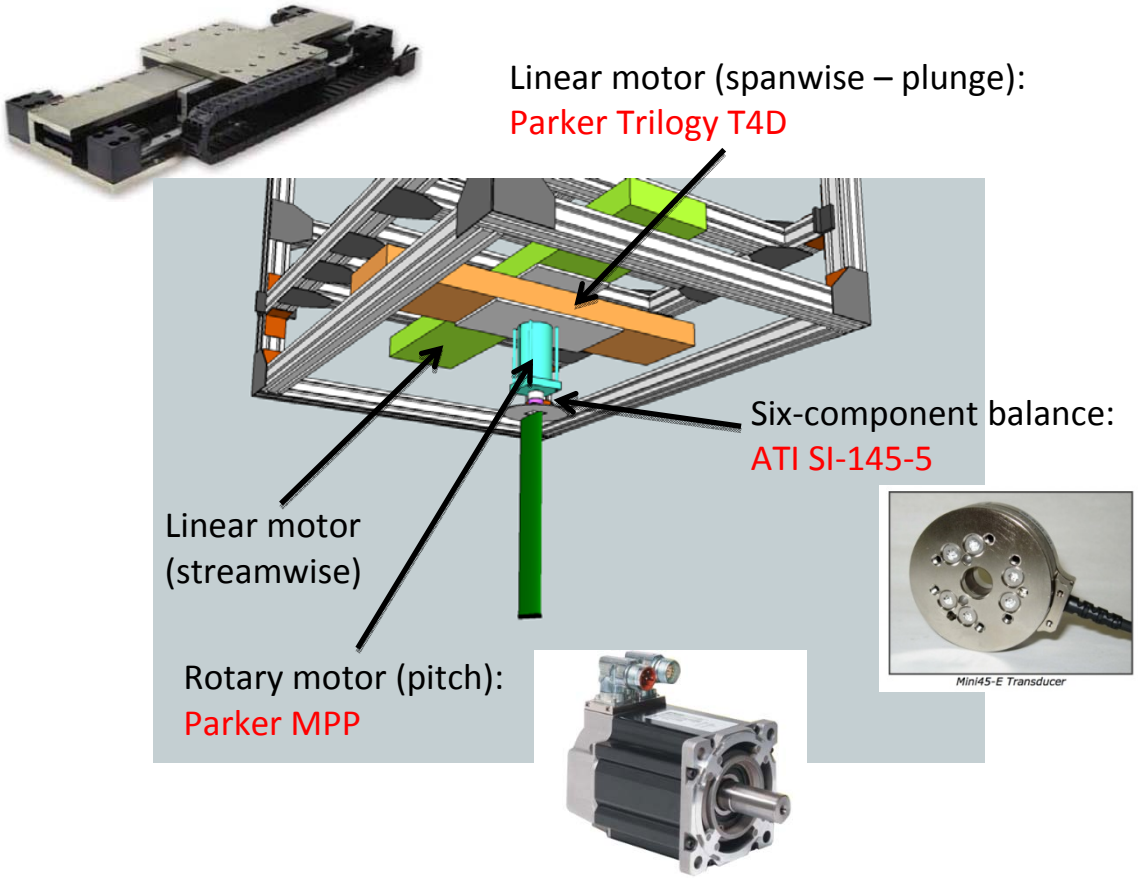

Figure 2. Details of the 3 DOF Motion System

IV.2. Airfoil Fabrication Using 3D Printing Methods

For the parts of the investigation focused on studying the effect of trailing edge flexibility, modern multi-material 3D printing technology is employed to fabricate the airfoil models. With this approach, the entire airfoil is fabricated using a 3D printer (Connex350) which is capable of printing objects using two materials, one rigid (VeroWhitePlus) and one flexible (TangoBlack), resulting in seamless integration of the rigid and flexible parts of the airfoil. Two different airfoil shapes are considered: a "long-tailed" and NACA-0009 airfoil (see Figure 3). The long-tailed airfoil consists of a rigid "head" portion that has a NACA 0036 profile, and a "tail" piece that is made from either the rigid or the flexible material. The chord of the airfoil is c = 30 mm, with the head stretching over 7.5 mm length. The airfoil's thickness ratio based on c is 0.09. To vary the flexibility of the airfoil, the thickness t of the tail is varied. The non-dimensional parameter G_1 typically used to characterize the structure flexibility is defined as:

$$G_1 = \frac{Et^3/(12(1-\nu^2))}{\rho U_\infty^2 c_2^3}, \qquad [1]$$

where E and ν are Young's modulus and Poisson's ratio for the tail material respectively, ρ is the fluid density, U_∞ is the freestream velocity and c_2 is the length of the tail (22.5 mm). Measurements conducted with this airfoil are done in ¼ scale water tunnel having a test section with a flow area of 15.2 cm × 15.2 cm. With the airfoil spanning the width of the test section, the airfoil's aspect ratio is approximately 5.

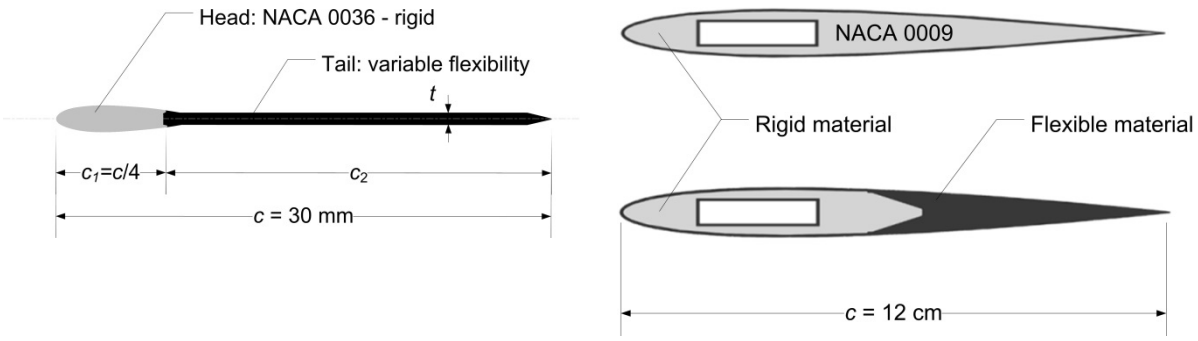

Figure 3. Illustration of the airfoil shapes employed in the unsteady airfoil studies in the present work: long-tailed (left) and NACA 0009 (right) airfoils. The rectangular cut-out in NACA 0009 airfoils is used to mount a support shaft

The other airfoil shape considered is NACA 0009 with chord length of 12 cm and aspect ratio of 2.8. A rigid and flexible versions of this airfoil are fabricated with the latter having the trailing flexible portion spanning 50% of the chord length. This airfoil is used in experiments in the full-scale, 61 cm × 61 cm, test facility.

IV.3. Velocimetry Techniques

The primary methodology empolyed for measurement of the velocity field are Particle Image Velocimetry (PIV) and Molecular Tagging Velocimetry (MTV). PIV is used for measurements in the wake of the long-tailed airfoil in the ¼-scale facility. These measurements are done using silver-coated hollow-glass-spheres (Potter Industries Inc. - SH400S20) seed with a mean diameter of about 20 μm. A 500 mW Lasiris Magnum SP Laser operating at a wavelength of 680 nm is employed to illuminate the glass spheres in the wake of the airfoil at about mid-span. A 12-bit 1392 pixel × 1024 pixel PCO Pixelfly QE camera controlled via Camware is used to record the PIV snapshots. The camera and laser pulses are synchronized using a Stanford Research Systems DG535 digital delay generator. One thousand pairs of images are acquired and processed for each case at the maximal frequency allowed by our setup (5 Hz). The PIV region of interest is limited to the wake region and is about 1.5 chord long in the streamwise (x) direction and 2 chord wide in the cross-stream (y) direction: see Figure 4. Interrogation of PIV images is done using the code by Thielicke and Stamhuis (http://pivlab.blogspot.com), yielding a velocity vector for every 16 pixel × 16 pixel interrogation volume (corresponding to $0.0283c \times 0.0283c$). Vector validation is implemented using a standard deviation and a local median check. The percentage bad vectorsis typically 2 – 5%. These are replaced via interpolation.

On the other hand, one- (1C) and two-component (2C) MTV measurements are employed for velocity measurements in the 0.61 m × 0.61 m water tunnel. The 1c-MTV measurements are predominantly used to characterize the separation bubble around a *stationary* SD 7003 airfoil. The details of these measurements are given in Olson *et al.* (2013). On the other hand, the 2C-MTV measurements are utilized in the experiments focused on studying the vortex wake structure behind rigid and flexible harmonically-pitching NACA 0009 airfoils. For these measurements, the beam from a Coherent COMPexPro 205 XeCl (308 nm) Excimer laser is directed through sheet forming optics, split using a 50/50 beam splitter and directed through

beam expanders and beam blockers before passing through the quartz windows of the test section to create a grid pattern with intersection angles of 105° (see Figure 5). Measurements are performed in a region downstream of the trailing edge and extending in the streamwise (x) direction from 0.1c to 0.7c, downstream of the trailing edge, and from -0.2c to 0.2c in the cross-stream (y) direction. The images are captured using a 14-bit 1392 × 1024 pixel PCO USB Pixelfly camera paired with a Nikkor 50 mm f/1.2 lens. The first image is acquired ~30 μs after the laser pulse, and the second is captured ~5.3 ms after the laser pulse. Correlation analysis is done on the two images using in-house Matlab code in order to extract velocity information. The resulting time series, from 1400 image pairs, are phase ordered and then averaged into 64 phase bins based on the acquisition (11.97 Hz) and motion frequencies.

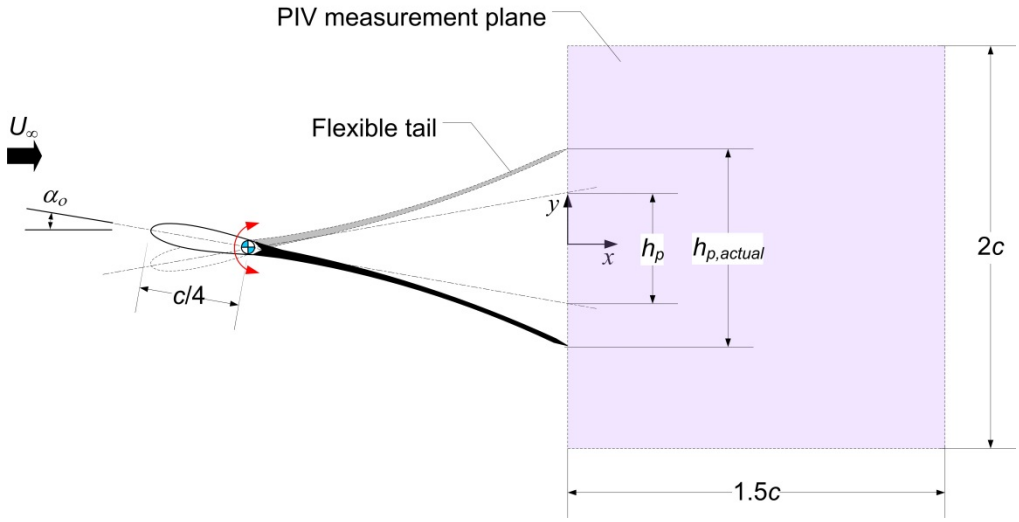

Figure 4. Illustration of the long-tailed airfoil motion trajectory and parameters, and the PIV measurement domain: U_∞ is the freestream velocity, α_o is the pitch angle oscillation amplitude, h_p is the *rigid* airfoil's trailing edge peak-to-peak deflection in the cross-stream (y) direction, and $h_{p,actual}$ is the corresponding deflection for the flexible airfoil

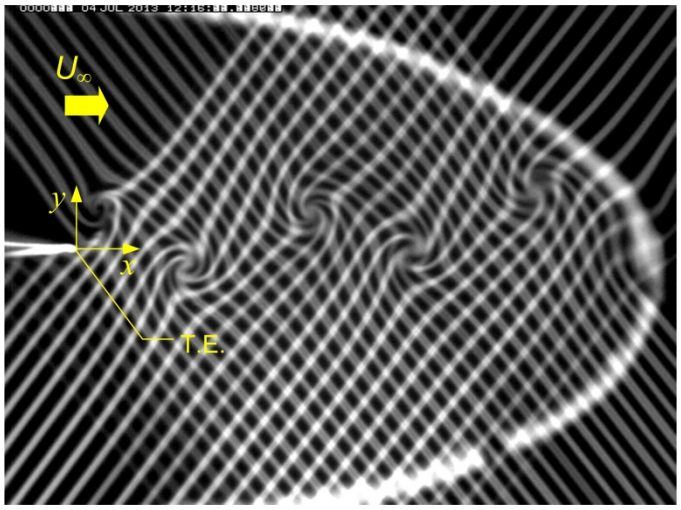

Figure 5. An image of a grid of tagged fluid molecules in the wake of a rigid NACA 0009 airfoil undergoing harmonic pitch oscillation around the ¼-chord point with reduced frequency k = 13.2 and Strouhal number St = 0.25. The grid is imaged with a long time delay relative to the initial excitation of the molecules by UV laser in order to visualize the wake vortex pattern

IV.4. Computational Methods

All simulations are performed employing the extensively validated high-order *FDL3DI* Navier-Stokes solver (described in more detail in Visbal and Gaitonde, 1999 & 2002), which was developed at the Computational Sciences Branch, AFRL Wright-Patterson Air Force Base. In this code, a finite-difference approach is used to discretize the governing equations, and all spatial derivatives are obtained employing a 6^{th}-order compact-differencing scheme. In order to eliminate high-frequency spurious components, an 8^{th}-order Pade-type low-pass spatial filtering operator (Visbal and Gaitonde, 1999 and 2002) is also incorporated. This filter is applied to the conserved variables along each transformed coordinate direction after each time step or sub-iteration. For transitional and turbulent flows, this filtering technique provides an effective implicit LES approach.

Initially, an O-mesh grid is used for the computation. However, as demonstrated in Figure 6, the grid is found to be coarse, causing superficially fast decay of vorticity in the airfoil wake. To remedy this problem, an overset grid with higher spatial resolution is used in the wake, yielding vorticity decay which agrees with the theoretical decay of a two-dimensional vortex having Gaussian core vorticity distribution.

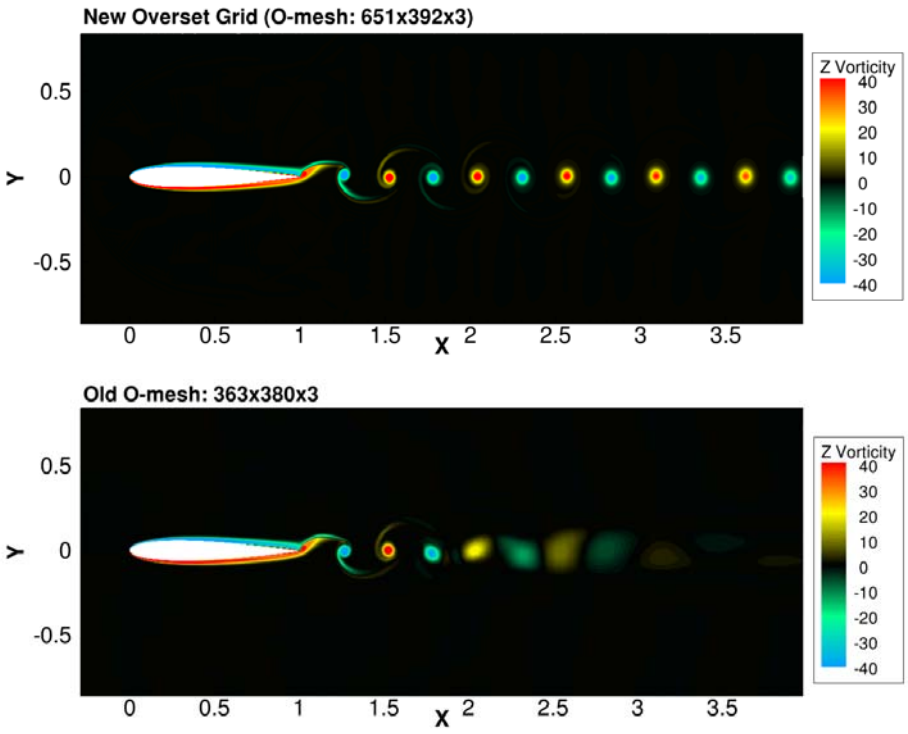

Figure 6. Demonstration of the effect of using an overset grid for computing the flow in the wake of a NACA 0012 airfoil undergoing harmonic pitch oscillation around ¼-chord point with $\alpha_o = 2°$, $k = 6.0$, $Re_c = 12{,}000$, and $M = 0.1$: non-dimensional vorticity ($\omega c/U_\infty$) maps with (top) and without (bottom) an overset grid. Flow is from left to right.

Since the simulation code is based on the governing equations for compressible flow, attention is also paid to the effect of the Mach number (M) on the simulation results. It is found that M could have a significant influence on the wake structure even for M values of order 0.1 and less. A particularly striking example is shown in Figure 7 for asymmetric oscillations of a NACA 0012 airfoil. As seen from the figure, the vortex structure in the far wake consists of only two opposite-sign vortices per wavelength for $M = 0.075$ and higher. This is inconsistent with experimental observations (also depicted in Figure 7), which show each wavelength to contain a positive vortex near the wake centerline and two negative vortices on opposite sides of the positive vortex. This type of structure could only be captured in the computations for $M = 0.05$ or less.

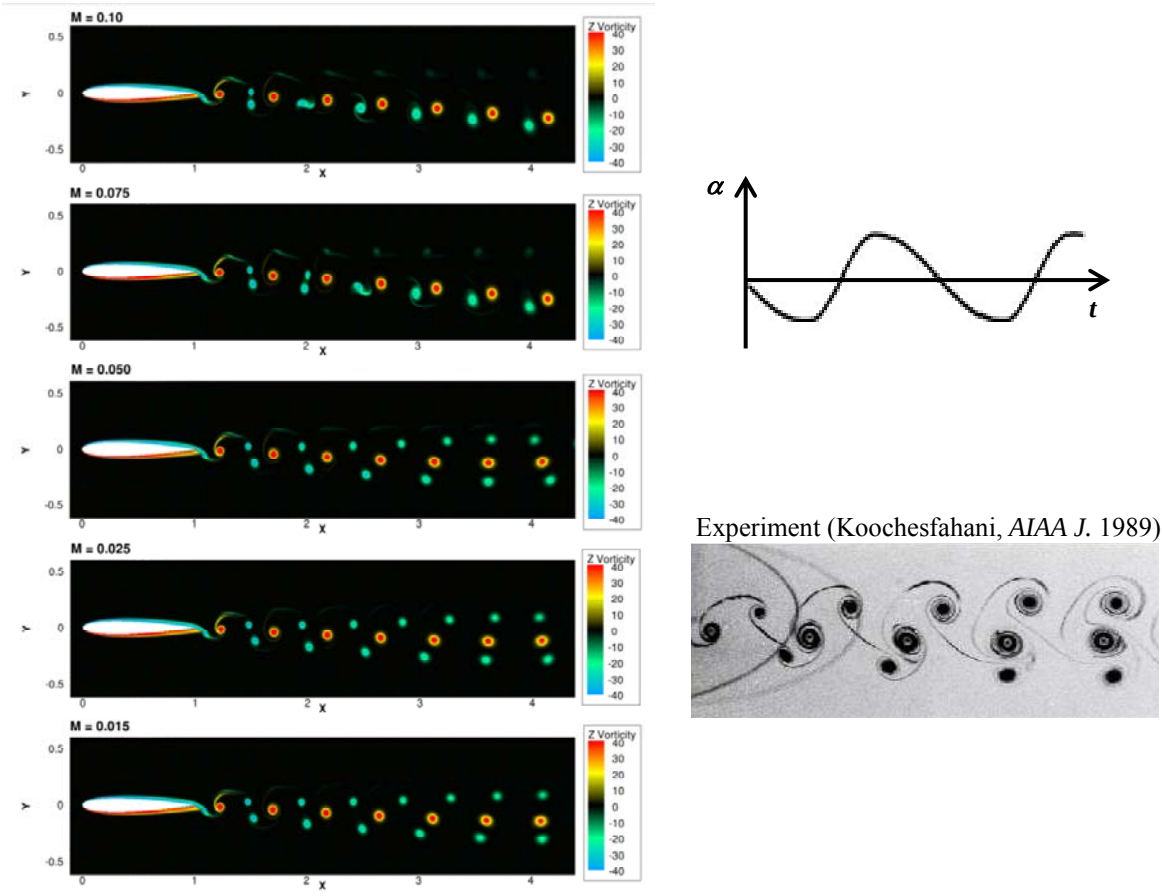

Figure 7. Demonstration of the effect of Mach number on the computed wake vortex structure of the flow in the wake of a NACA 0012 airfoil undergoing asymmetric pitch oscillation around ¼-chord point with $\alpha_o = 2°$, $k = 6.68$ and $Re_c = 12{,}000$: angle of attack variation (top right) exhibits faster pitch-up (38% of oscillation period) than pitch-down motion, computed non-dimensional vorticity ($\omega c/U_\infty$) maps (left) for different Mach numbers (with Mach number increasing from bottom to top), and dye flow visualization (bottom right). Flow is from left to right for experimental and computational results.

IV. Results

IV.1. Low-Reynolds-Number Separation over SD 7003 Airfoil

Coordinated computational and experimental efforts are undertaken to investigate the separation bubble associated with the low Reynolds number flow ($Re_c = 2\times10^4 - 4\times10^4$) around an SD7003 airfoil (Figure 8) at different angles of attack. Previous work has already demonstrated a great deal of variability in the separation and reattachment locations (X_s and X_r, respectively) measured under the same nominal flow conditions but in three different test facilities. In the present work, the difficulty in accurately determining the separation and/or reattachment locations of separation bubbles over airfoils at low Reynolds number is further underlined where *even* results from the coordinated experiments and computations at the same Reynolds number and angle of attack can exhibit substantial differences: see Figure 9. By methodically examining the experimental uncertainty in determination of the separation and reattachment locations, we are able to identify various factors which render accurate characterization of the separation bubble at low Reynolds number challenging. These factors are: (I) the ability to determine the

angle of attack accurately, (II) the sensitivity of the flow to relatively small Reynolds number variation under certain conditions, (III) the required near-wall measurement spatial resolution, and (IV) the variation in freestream turbulence intensity from one test facility to another. Details of this work can be found in Olson (2011), Olson *et al.* (2011) and Olson *et al.* (2013).

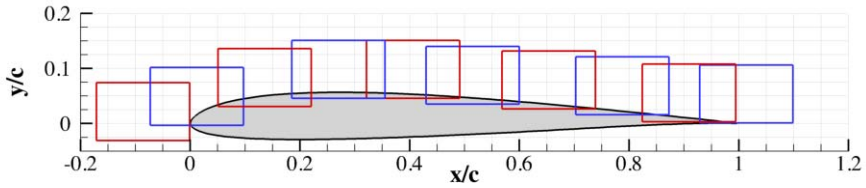

Figure 8. Illustration of the SD7003 airfoil shape, along with ten overlapping fields of view used to capture the near surface flow using high resolution 1c-MTV measurements. Additional fields of view are added above these depicted to capture the entire shear layer, as needed, and the freestream conditions

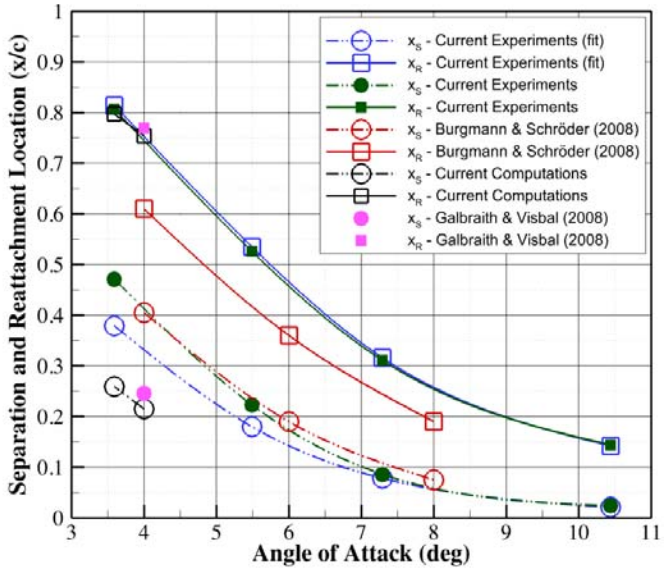

Figure 9. Comparison of separation and reattachment locations obtained from different studies of the flow over an SD7003 airfoil at a nominal $Re_c = 4\times10^4$. A square symbol is used for reattachment location whereas a circle is used for separation location data. Splines are used to connect points to highlight the trends. Current results are obtained in two different ways: (I) from the first reliable velocity measurement above the surface; (II) using a polynomial fit to the reliable data and the no-slip boundary condition at the wall.

IV.2. Effect of TE Flexibility on Wake Vortex Pattern

IV.2.a. Studies of the long-tailed airfoil model. In these studies, PIV measurements are conducted in the wake of harmonically pitching airfoils possessing a flexible 'tail' (see Figure 4 and associated discussion), the structural flexibility of which is varied over three orders of magnitude. Data are obtained for different oscillation amplitudes and frequencies and chord Reynolds number of Re_c = 1950. The focus of the data analysis is on extracting the circulation (Γ) and streamwise and cross-stream spacing (a and b respectively) of the vortices shed into the wake: see Figure 10 for definitions. The influence of the airfoil flexibility on how these parameters vary with change in the amplitude and frequency of oscillation is investigated.

The results show that at a given reduced frequency, an optimum airfoil flexibility exists which results in the earliest switch in the wake vortex pattern from classical to reverse von Kármán street (i.e. b switching sign from negative to positive) with increasing oscillation amplitude. This optimum flexibility shifts towards stiffer tails with increasing reduced frequency. More interestingly, a good correlation for all airfoils examined is found for the variation of b/c with Strouhal number ($St = fh_p / U_\infty$; f is oscillation frequency and h_p is as defined in Figure 4) if the latter is defined using the *actual* oscillation amplitude of the trailing edge ($St_{te} = fh_{p,actual} / U_\infty$; $h_{p,actual}$ is as defined in Figure 4). These results are depicted in Figure 11. Similar correlations are also found for the dependence of the circulation, streamwise spacing and convection velocity when using the latter definition of the Strouhal number. Details may be found in Monnier *et al.* (2013).

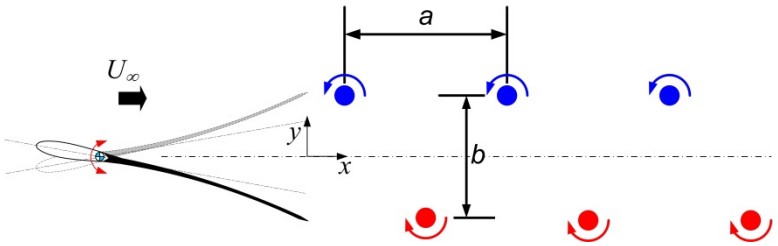

Figure 10. Definition of geometrical parameters of the vortex pattern in the wake of the long-tailed airfoil

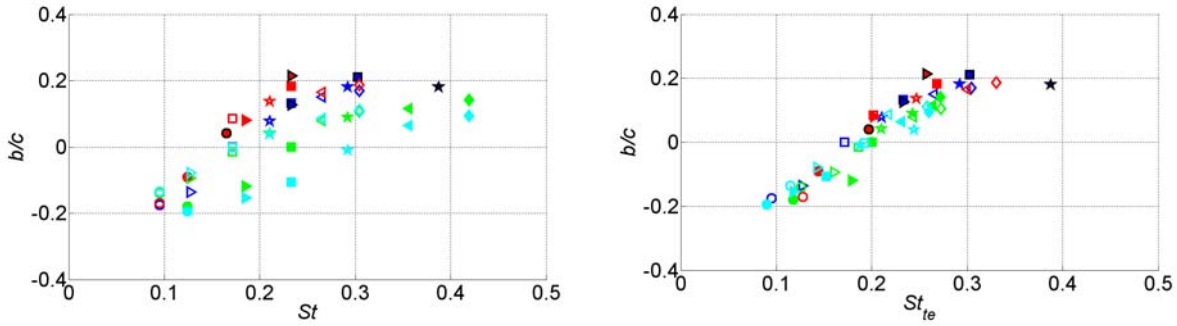

Figure 11. Dependence of b/c on St (left) and St_{te} (right) for the long-tailed airfoil. Colors represent airfoil flexibility: blue: rigid, red: $G_1 = 5.6$, green: $G_1 = 1.4$, cyan: $G_1 = 0.7$. Symbols represent amplitude α_o: circle: 2°, right triangle: 3°, square: 4°, star: 5°, left triangle: 6°, diamond: 7°. Symbol filling represents frequency: open symbols: $k = 4.89$, filled symbols: $k = 6.19$, filled symbol with black outline: $k = 7.74$. b/c uncertainty is estimated to be $\pm 0.028c$ (corresponding to ± one PIV grid spacing).

IV.2.b. Preliminary studies of the NACA-0009 airfoil model. This component of the investigation is still ongoing. The results shown here represent some preliminary observations of differences between the wake vortex pattern observed in the wake of a rigid and flexible NACA-0009 airfoils, obtained using 2C-MTV measurements at $Re_c = 12{,}500$. For the case examined both airfoils undergo pitch oscillation around ¼-chord point with an amplitude of 2.25 degrees and reduced frequency of $k = 13.2$ ($St = 0.25$). The trailing edge (TE) displacement of both airfoils is measured from the MTV images and the results are shown in Figure 12. The flexible airfoil TE movement is found to have 27% larger amplitude than the rigid airfoil and to exhibit a phase lag of 34 degrees. The vorticity field for both airfoils is shown in Figure 13 at the same phase of the oscillation cycle. Using these results, parameters of the wake vortex pattern are

computed and compared in Table 1. As can be seen from the table, the airfoil flexibility results in larger cross-stream vortex spacing and vortex circulation (even though the imposed airfoil motion in both cases is the same). These differences (i.e. increased *b/c* and Γ) , which are clearly related to the different boundary condition associated with the deformation of the flexible airfoil (e.g. the difference in TE motion seen in Figure 12), are expected to result in producing larger mean thrust on the airfoil. In fact, the mean streamwise force coefficient (Cf) is computed for these two cases using the momentum integral equation (see Bohl and Koochesfahani (2009) for the details), and the results are shown in Figure 14 along with data from an earlier study by Bohl (2002), which covered a substantially wider range of oscillation frequencies. As can be seen from the figure, the flexible airfoil does in fact results in a larger mean thrust coefficient (specifically 0.105 in comparison to 0.046: a 2.3 fold increase). It is also interesting to note how the current Cf data along with data from Bohl (2002) seem to collapse on a single trend line when plotted versus the Strouhal number based on the actual TE oscillation amplitude. These results are consistent with the conclusions made in section IV.2.a. regarding the dependence of the wake vortex parameters of the long-tailed airfoil with different tail flexibilities on the Strouhal number.

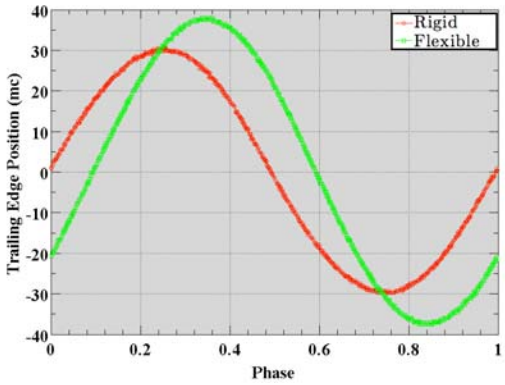

Figure 12. Measured trailing edge deflection of the rigid (red trace) and flexible (green trace) NACA-0009 airfoils over one oscillation cycle. Deflection is shown in units of "milli-chord" (mc)

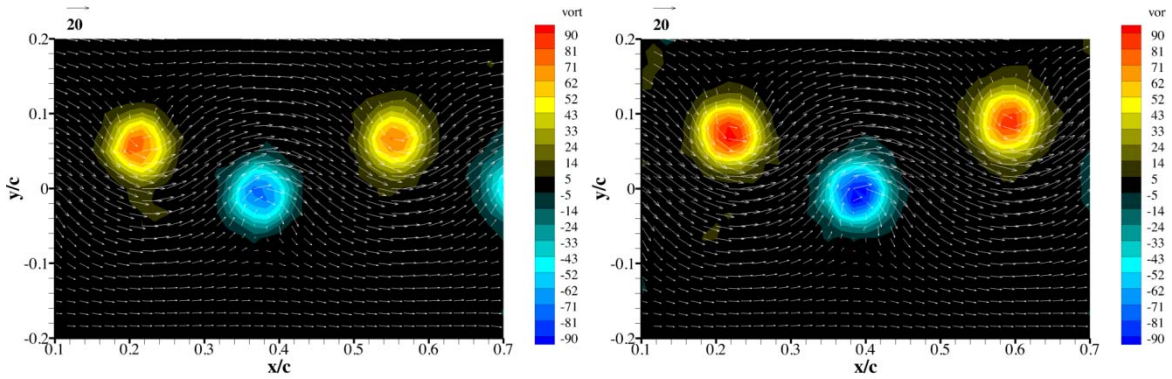

Figure 13. Velocity field superposed on top of the vorticity field measured in the wake of the rigid (left) and flexible (right) NACA-0009 airfoils at the same phase of the oscillation cycle. The color bar indicates the vorticity magnitude in s^{-1}, and the arrow above the top-left corner of each plot represents the freestream velocity of 20 cm/s

Table 1. Comparison between the wake vortex parameters for the rigid and flexible NACA-0009 airfoils

Parameter	Rigid Airfoil	Flexible Airfoil	Difference
b/c	0.068	0.088	28%
Peak Vorticity (s^{-1})	75	91	21%
Γ (cm^2/s)	52	68	30%

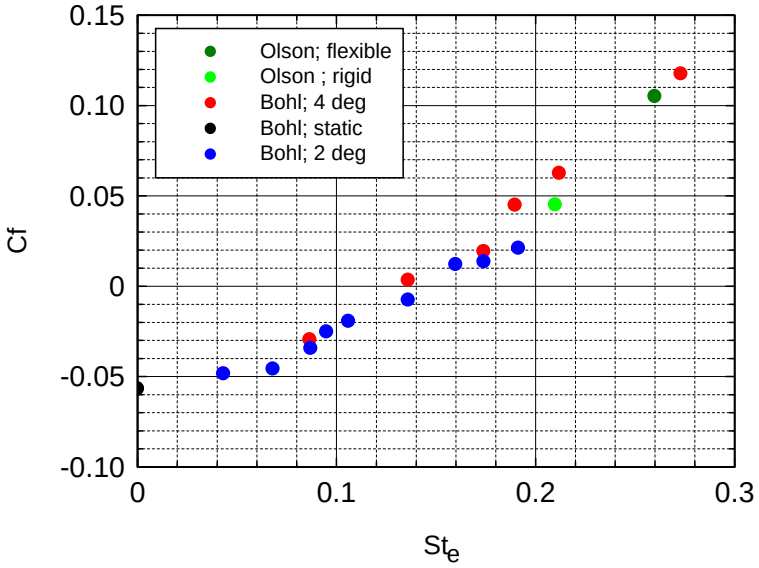

Figure 14. Comparison of the mean streamwise force coefficient obtained from the current results (Olson) with data obtained by Bohl (2002) in the wake of NACA-0012 airfoil exhibiting harmonic pitch oscillation around the ¼-chord point

IV.3. Reynolds Number Effects

Our low Reynolds number data at $Re_c \approx 2{,}000$ (Monnier, *et al.* 2013) indicate that the crossover reduced frequency for the vortex arrangement switch (i.e. from wake to jet profile) occurs at $k \approx 7.8$ for rigid airfoil at amplitude of $A = 2°$. This is significantly higher than $k \approx 5.9$ previously measured as the crossover condition at $Re_c \approx 12{,}600$ for the same oscillation amplitude (Bohl and Koochesfahani, 2009). As we will show below, similar Reynolds number effects also occur in connection to the conditions needed for thrust generation.

To examine the Reynolds number effects, CFD studies were carried out using the FDL3DI solver of Visbal at the AFRL. Figure 15 depicts the computed crossover reduced frequency k for switch in vortex arrangement in comparison with existing limited data from both experiments and other computations. A clear Reynolds number dependence is revealed in this figure. We note the very good agreement between the crossover k from our current CFD results and our previous experiments. However, notable differences from previous computional results are also observed.

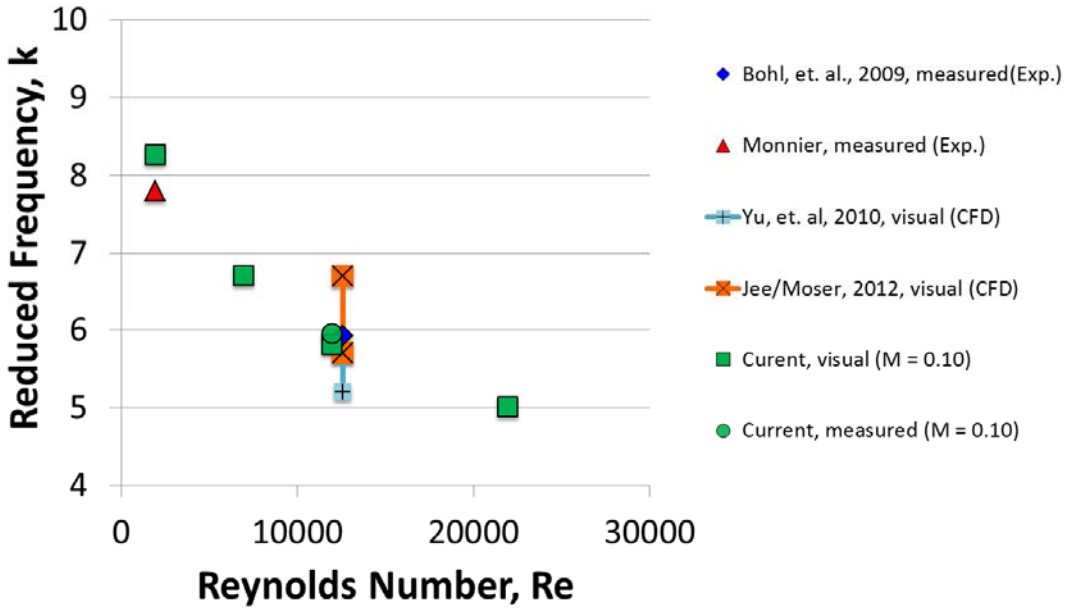

Figure 15. Reynolds number dependence of crossover reduced frequency k for the vortex arrangement switch (NACA 0012; Oscillation amplitude $A = 2°$).

The computed influence of Reynolds number on the crossover reduced frequency k for the drag-to-thrust switch is shown in Figure 16. Consistent with the previous finding of Bohl & Koochesfahani (2009), the values of k for the drag-to-thrust switch are higher than those for switch in vortex arrangement. Note that the drag-to-thrust crossover reduced frequency decreases by about a factor of two (from 13.91 to 6.86) as the Reynolds number increases from 2,000 to 22,000. For reference, we would mention that the Euler calculations of Ramamurti & Sandberg (2001) estimated the drag-to-thrust crossover to be at $k \approx 3.35$ in the inviscid limit, significantly lower than the range of values for the viscous cases studied here.

Figure 17 illustrates the comparison of our data with those in the literature in terms of the crossover Strouhal number St for the drag-to-thrust switch versus Reynolds number. Using the Strouhal number, which is based on the peak-to-peak trailing edge amplitude, allows us to compare results across different pitch oscillation amplitudes. The results in Figure 17 are instructive in two ways. First, our computed results show an excellent quantitative agreement with our previous experiment (Bohl and Koochesfahani, 2009) and also the estimate provided by our vortex array model (Naguib, *et al.*, 2011) applied to incomplete data of Koochesfahani (1989). Second, there is significant disagreement among the various computational studies in their prediction of the crossover frequency, in some cases by nearly a factor of two.

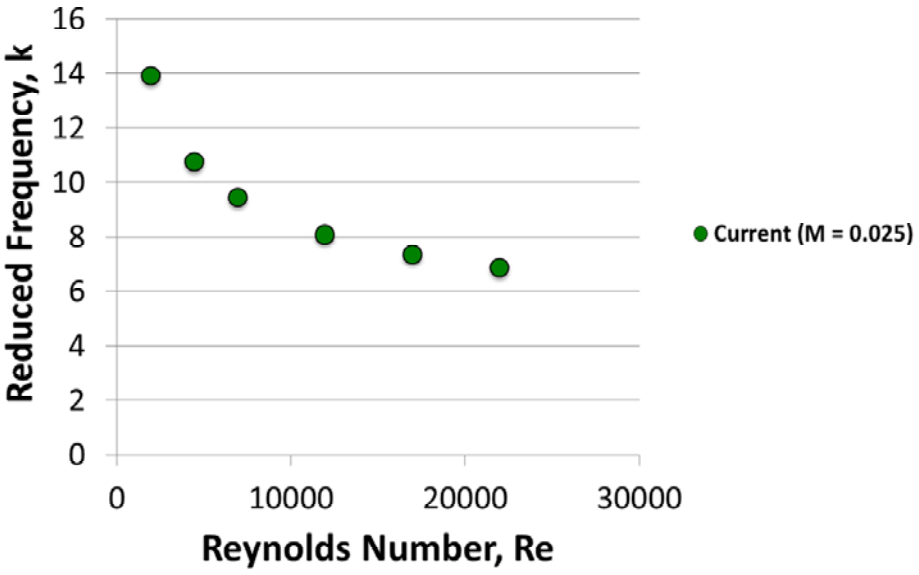

Figure 16. Evidence for Reynolds number dependence of crossover reduced frequency for the drag-to-thrust switch (NACA 0012; Oscillation amplitude $A = 2°$).

We note that the quantitative agreement in Figure 17 between our current CFD results and data from our previous experiments required significant attention to numerical issues (resolution, grid generation, convergence, etc.). A major difficulty in assessing the adequacy of the various computational studies of unsteady low-Re airfoils have been a lack of detailed quantitative data from experiments with conditions matched to the computations, and comparisons/validations are often made on a qualitative basis. Qualitative comparisons seem to be prevalent even when appropriate experimental data are, in fact, available.

The Reynolds number effects shown in Figures 15-17 have not been previously addressed, to our knowledge, but they have important implications. They may play a partial role in the disagreements that are routinely noted between CFD results and experiments. More importantly, they indicate that the airfoil operating condition needed for generation of thrust is unique to the particular value of chord Reynolds number.

The results of this effort are being packaged in a manuscript for journal submission.

IV.4. Development of MTV-based Wall-Shear and -Pressure Measurement Technique

Evaluation of the Navier-Stokes equations at the surface of a moving solid object leads to the following expression for the wall pressure distribution along the surface:

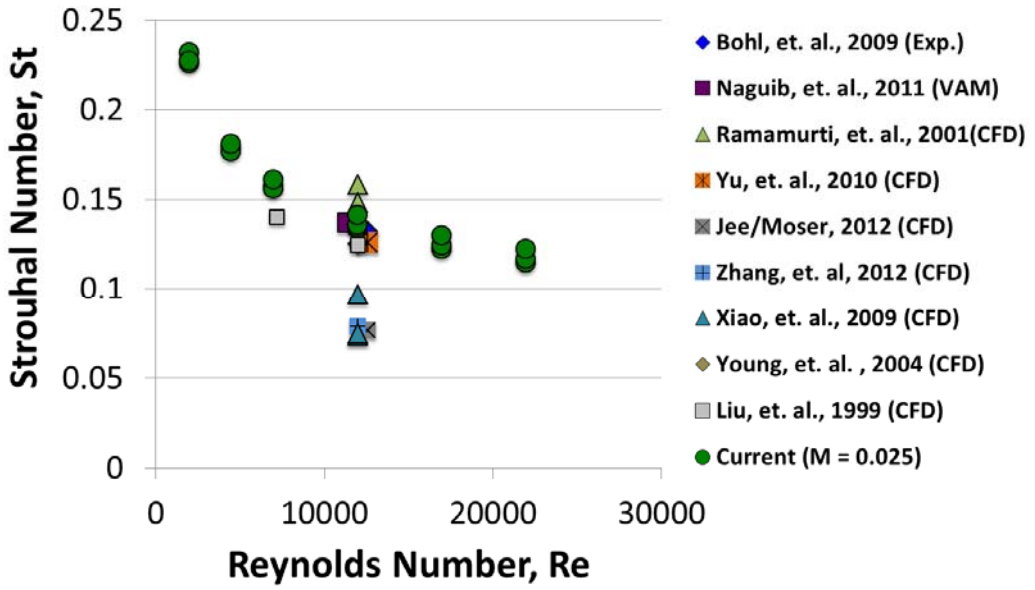

Figure 17. Evidence for Reynolds number dependence of crossover Strouhal number for the drag-to-thrust switch (NACA 0012).

$$p_w(\xi) - p_w(\xi_o) = \int_{\xi_o}^{\xi} \left\{ \left[-\rho a_{w;\xi} + \mu \left. \frac{\partial^2 u_\xi}{\partial \xi^2} \right|_w \right] + \mu \left. \frac{\partial^2 u_\xi}{\partial \eta^2} \right|_w \right\} d\xi \qquad [2].$$

In this expression η, ξ are coordinates normal and tangent to the surface, $p_w(\xi_o)$ is a "boundary condition" specifying the pressure at an arbitrarily selected point on the wall, $a_{w;\xi}$ is the surface-tangent component of the wall acceleration, u_ξ is the flow velocity component in the ξ direction and μ is the dynamic viscosity. Inspection of Equation [2] shows that, given a prescribed airfoil/wing motion trajectory and measurement of the wall pressure at an arbitrary single reference point on the surface (e.g. at the leading edge), the pressure distribution around the airfoil, at a given spanwise location, can be obtained from the measurement of $\left. \frac{\partial^2 u_\xi}{\partial \eta^2} \right|_w$ over the circumference of the airfoil/wing.

In our work, we take advantage of the high spatial (pixel level) resolution of the single-component, line-tagging mode of MTV (1c-MTV) for near-wall measurements. The near-wall capability is due to both the molecular nature of MTV and also to little/no wall glare. By orienting the line tags normal to the surface (a condition imposed for convenience but can be relaxed), 1c-MTV essentially provides a "continuous" distribution of u_ξ in the η direction. Thus,

the curvature of the line tags at the wall is physically $\left.\frac{\partial^2 u_\xi}{\partial \eta^2}\right|_w$ (after correction for the wall-normal velocity due to the motion of the airfoil as mentioned above). In addition to measurements of the surface pressure, the line-tagging MTV mode can be used to obtain the ξ component of the wall shear stress $\tau_{w;\xi}$. In this case, the slope of the line tags at the wall will be used to calculate the shear stress using:

$$\tau_{w;\xi} = \mu \left.\frac{\partial u_\xi}{\partial \eta}\right|_w \qquad [3]$$

An initial study was carried out to assess the accuracy of computing the second derivative of the velocity profile at the wall from MTV data and how it depends on the spatial resolution of the measurement, the streamwise pressure gradient, the boundary layer thickness, and the order of accuracy of the numerical derivative scheme. This study utilized the Falkner-Skan boundary layer solutions as a model for boundary layers developing under non-zero pressure gradient, along with the CFD solution of the flow over an airfoil (SD7003) for an analysis of a complete flow field. The results of this work confirmed the feasibility of surface pressure estimation from multi-line MTV measurements and also established the various constraints that impact the accuracy of the approach.

While the line-tagging mode of MTV provides highly resolved measurements of a single component of the velocity normal to the line tags, the accuracy of the measured velocity can suffer from the "V-bias" problem. This problem is connected with the component of the velocity that might exist along the line tags, causing an ambiguity in uniquely determining the displacements of the 'individual fluid particles' comprising the (*continuous*) tagged line. A detailed analysis of the error led to a novel correction method involving the acquisition of MTV images at multiple time delays. The effectiveness of this 'multi-time-delay' approach for correcting the 1c-MTV data has been validated experimentally and the results appear in a recent journal publication (Hammer, *et al.*, 2013)

We have recently carried out a quantitative experimental demonstration of the MTV-based capability for measuring surface pressure and shear stress distributions. The experiments considered the flow around a stationary circular cylinder in a water tunnel at a cylinder Reynolds number (based on diameter) of *Re* = 6,000. For this flow field, Equation [2] reduces to the following expression.

$$p_w(\xi) - p_w(\xi_o) = \int_{\xi_o}^{\xi} \left\{ \mu \left.\frac{\partial^2 u_\xi}{\partial \eta^2}\right|_w \right\} d\xi \qquad [4]$$

Figure 18 shows a composite image of the tagged regions acquired 7 ms after initial tagging. The laser beam was arranged to exit the surface of the transparent circular cylinder in a radial direction at a series of angular locations. The wall normal spatial resolution was 37 μm, resulting in about 27 points/mm in the velocity profile. Two samples of the measured mean velocity

profiles are indicated in this figure for the two selected angular positions. The highly resolved nature of the velocity data near the surface is noted.

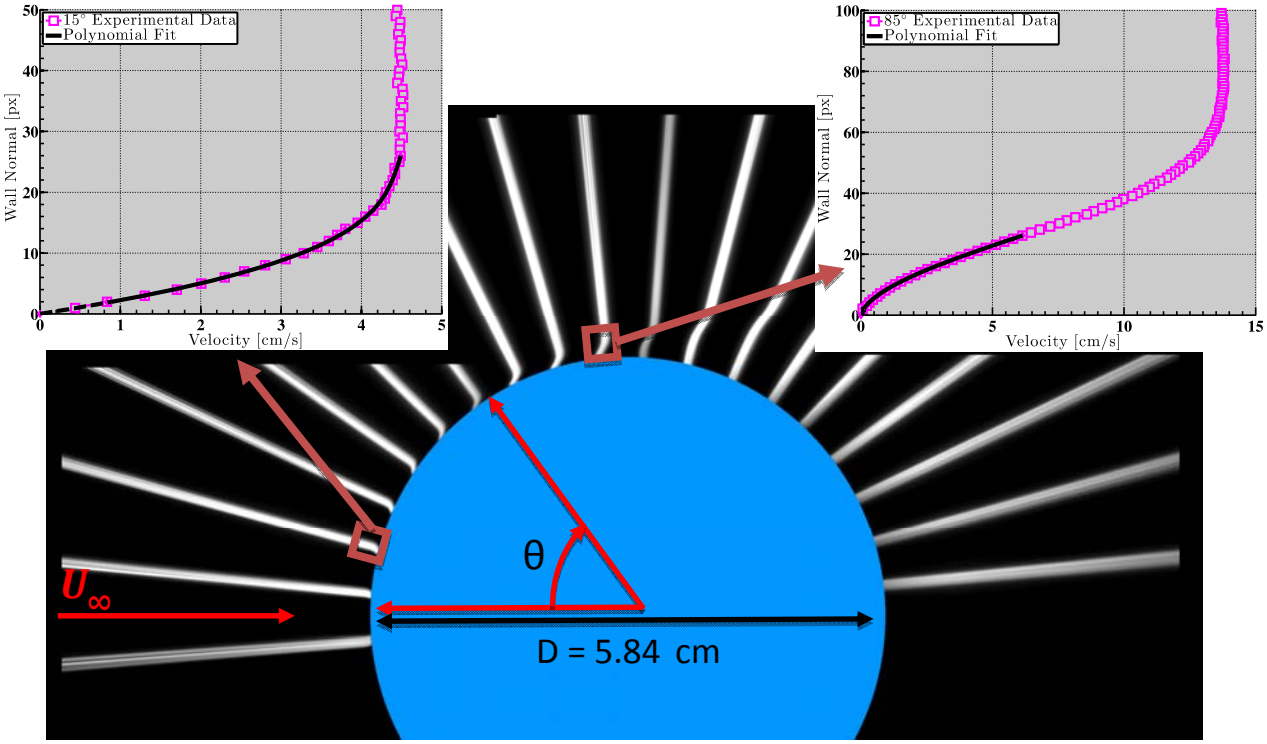

Figure 18. Composite delayed image of the radially tagged regions around the circular cylinder at *Re* = 6,000. The delayed image is acquired 7 ms after initial tagging. Wall normal resolution is 37 μm (27 points/mm). The two insets show the measured velocity profiles at the two particular angular locations marked.

A 3rd order polynomial fit to near wall data was used to estimate the second and first order derivatives of the velocity at the surface. The second order derivative was used in conjunction with Equation [4] to determine the surface pressure distribution, along with specifying the boundary condition at the front stagnation point. Results are shown in Figure 19 in terms of the distribution of surface pressure coefficient C_p. We can see that our results at *Re* = 6,000 are in very good agreement with published results at neighboring values of Reynolds number.

Comparison of the measured surface shear stress distribution with literature data is more challenging since this variable is often not included in publications. However, we were able to obtain from the Visbal group at AFRL the shear stress data for the computations reported in Rizzetta & Visbal (2009) for *Re* = 10,000. To scale their shear stress data to the Reynolds number of our experiment (*Re* = 6,000), we note that for zero pressure gradient (Blasius) boundary layers the surface friction coefficient C_f scales as $1/\sqrt{\mathrm{Re}}$. This scaling also holds for non-zero pressure gradient (Falkner-Skan) boundary layer solutions. Since according to Figure 19 the pressure distribution is very weakly dependent on the Reynolds number, over the range *Re* = 6,000 – 10,000, the boundary layer evolves under very similar external pressure gradient and we expect the $1/\sqrt{\mathrm{Re}}$ scaling for C_f to continue to hold. The measured surface friction coefficient

C_f and that arrived at from the computations, using the scaling just described, are shown in Figure 20. We point out the excellent agreement between the data sets in this figure.

The results of this development are being presented at the 2013 meeting of the APS/DFD and a journal manuscript is also being prepared.

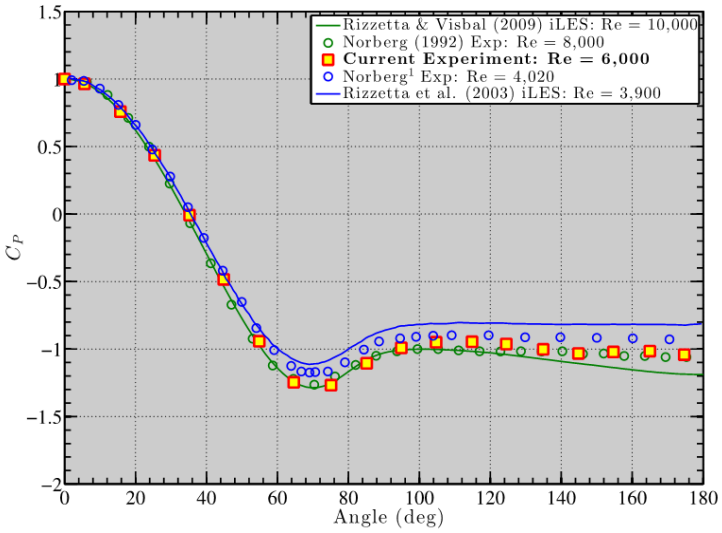

Figure 19. Comparison of the measured circular cylinder surface pressure coefficient against literature data.

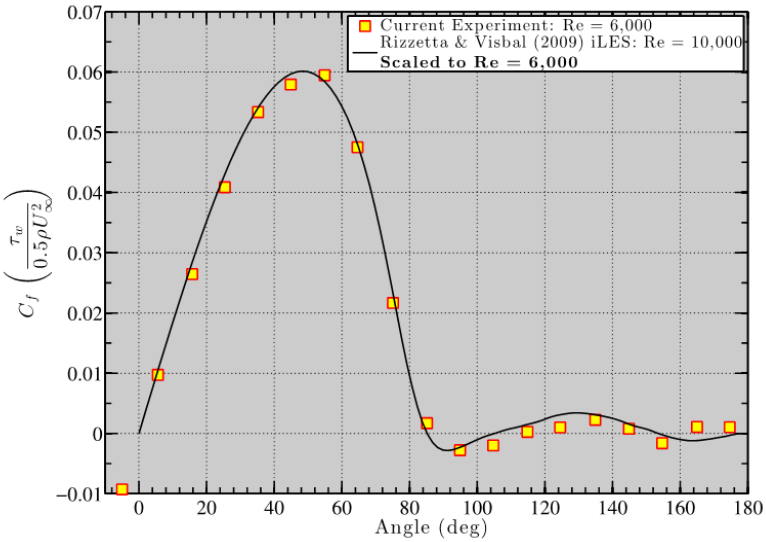

Figure 20. Comparison of the measured circular cylinder surface shear stress distribution against the computational results. Scaling according to $1/\sqrt{\mathrm{Re}}$ was used to transform the computational results at *Re* = 10,000 to the Reynolds number of the experiment.

V. Summary

A coordinated experimental and computational investigation is carried out to study the fundamental aerodynamics of oscillating airfoils in the chord Reynolds number range of 2×10^3 – 6×10^4. The objective of the investigation is to establish the connection between the airfoil motion trajectory, the trailing edge flexure, the time history of vorticity flux at the trailing edge, the pattern of shed vorticity and its evolution, and the conditions for generation of thrust/drag and lift. The following list summarizes the key findings of the study:

- In computing the flow over unsteady airfoils, special attention must be paid to the computational grid resolution if one is to study the characteristics of the wake vortex pattern. The resolution requirement in the wake could be more stringent than required to capture the force on the airfoil without worrying about the connection to the wake behavior. In the present study, the grid resolution requirements in the wake are met using a fine Cartesian grid superposed on top of an O grid in the wake of the airfoil.
- When using a compressible-flow code to compute the flow over unsteady airfoils, compressibility may have substantial influence on the results even at Mach numbers as low as 0.1 or lower. The influence is particularly significant at high reduced frequency. A Mach number-independent solution as $M\rightarrow0$ (or one that is consistent with experimental observations) should be sought systematically if the target application is that involving incompressible flow.
- Experimental determination of the characteristics of separation bubbles over airfoils at low Reynolds number is challenging. The factors contributing to this difficulty have been identified and examined systematically in the present work.
- The wake vortex characteristics and the mean thrust coefficient of rigid and flexible airfoils are similar if characterized using the Strouhal number based on the actual oscillation amplitude of the trailing edge, rather than using the Strouhal number based on the imposed motion.
- For a given oscillation reduced frequency, an optimum trailing edge flexibility exists, which will result in the switch in the vortex wake pattern to the "reversed" von Kármán vortex street at the smallest possible oscillation amplitude. This optimum flexibility is such that the higher the reduced frequency of oscillation, the stiffer the structure of the optimum trailing edge material.
- The Reynolds number has a very important, yet unrecognized hitherto, influence on the reduced frequency and Strouhal number at which the wake vortex pattern assumes the "reversed" von Kármán vortex street configuration and the net force acting on the airfoil switches from drag to thrust. This effect is documented systematically in the present work and the underlying physics leading to this influence is currently under examination.
- New multi-time-delay-based method is introduced for improvement of the accuracy of high-resolution (pixel level) one-component Molecular Tagging Velocimetry (1c-MTV). The interest in 1c-MTV is motivated by the suitability of the method for conducting near-wall boundary-layer-resolved measurements. This suitability is capitalized upon in the present investigation in order to extract the wall-shear-stress and wall-pressure information. The approach is validated by conducting measurements over a cylinder in cross flow, and comparing the results against existing experimental and computational studies of the same flow. This approach for measuring the wall shear stress and pressure provides a clever solution for measuring these quantities over flexible and moving surfaces where such

measurements are challenging to obtain using surface mounted sensors, pressure taps, or other traditional means. A particularly significant area of application of the new technique is in aeroelastic problems where access to velocity field information and the concurrent stresses acting on a moving structure would yield tremendous insight.

References

Anderson, J. M., Streitlien, K., Barrett, D. S. And Triantafyllou, M. S. [1998] "Oscillating foils of high propulsive efficiency," *J. Fluid Mech*., **360**, 41-72.

Bohl, D.G. [2002] "Experimental study of the 2-D and 3-D structure of a concentrated line vortex array," *Ph.D. Thesis*, Michigan State University, East Lansing, MI.

Bohl, D. G. and Koochesfahani, M. M. [2009] "MTV Measurements of the Vortical Field in the Wake of an Airfoil Pitching at High Reduced Frequency," *J. Fluid Mech*., **620**, 63-88.

Djojodihardjo, R. H. and Widnall, S. E. [1969] "A numerical method for the calculation of nonlinear, unsteady lifting potential flow problems," *AIAA J*., Vol. 7, No. 10, 2001-2009

Giesing, J. P. [1968] "Nonlinear two-dimensional unsteady potential flow with lift," *J. Aircraft*, **5(2)**, 135-143.

Hammer, P., Pouya, S., Naguib, A., and Koochesfahani, M. [2013] "A Multi-Time-Delay Approach for Correction of the Inherent Error in Single-Component Molecular Tagging Velocimetry," *Meas. Sci. Technol*., **24**, 105302 (11pp) (DOI:10.1088/0957-0233/24/10/105302)

Jee, S., and Moser, R.D. [2012] "Conservative Integral Form of the Incompressible Navier-Stokes Equations for a Rapidly Pitching Airfoil," *J. Comp. Phys.*, **231**, 6268-6289.

Koochesfahani, M. M. [1989] "Vortical patterns in the wake of an oscillating airfoil," *AIAA J*., **27(9)**, 1200-1205.

Koochesfahani, M. M. and Bohl, D. [2002] "Molecular tagging visualization and velocimetry of the flow at the trailing edge of an oscillating airfoil," *Proceedings of the 10th International Symposium on Flow Visualization*, Kyoto, Japan, Paper No. F0453.

Lai, J. C. S. and Platzer, M. F. [1999] "Jet characteristics of a plunging airfoil," *AIAA J*., **37(12)**, 1529-1537.

Lighthill, J. [1975] Mathematical Biofluiddynamics, SIAM, Philadelphia, 1975.

Liu, H. and Kawachi, K. [1999] "Numerical study of undulatory swimming," *J. Comp. Phys.*, **155**, 223-247.

McCroskey, W.J. [1982] "Unsteady airfoils," *Annual Review of Fluid Mechanics*, **14**, 285.

Monnier, B., Naguib, A. M., and Koochesfahani, M. M. [2013] "Investigation of the Wake Vortex Pattern of Rigid and Flexible Airfoils Undergoing Harmonic Pitch Oscillation," *AIAA* Paper No. AIAA 2013-0841.

Naguib, A. M., Vitek, J., and Koochesfahani, M. M. [2011] "Finite-Core Vortex Array Model of the Wake of a Periodically-Pitching Airfoil," *AIAA J*., **49(7)**, 1542-1550.

Olson, D., "Facility And Flow Dependence Issues Influencing the Experimental Characterization of a Laminar Separation Bubble at Low Reynolds Number," M.S. Thesis, Mechanical Engineering Dept., Michigan State University, East Lansing, MI, 2011.

Olson, D., Katz, A., Naguib, A.M., Koochesfahani, M.M., Rizzetta, D.P. and Visbal, M. [2011] "An investigation of the effect of freestream turbulence on the laminar separation bubble on an SD7003 airfoil," AIAA Paper 2011-395, *49th AIAA Aerospace Sciences Meeting*, Orlando, FL.

Olson, D.A., Katz, A.W., Naguib, A.M., Koochesfahani, A.M., Rizzetta, D.P. and Visbal M.R. [2013], "On the challenges in experimental characterization of flow separation over airfoils at low Reynolds number," *Exp. Fluids* **54 (2)**, DOI 10.1007/s00348-013-1470-1.

Ramamurti, R. & Sandberg, W. [2001] "Simulation of flow about flapping airfoils using finite element incompressible flow solver," *AIAA J.*, **39**, 253-260.

Rizzetta, D. and Visbal, M. [2009] "Large Eddy Simulation of plasma-based control strategies for bluff body flow," *AIAA J.*, **47(3)**, 717-729.

Shyy, W., Lian, Y., Tang, J., Liu, H., Trizila, P., Stanford, B., Bernal, L., Cesnik, C., Friedmann, P, and Ifju, P. [2008] "Computational aerodynamics of low Reynolds number plunging, pitching and flexible wings for MAV applications," *AIAA Paper No. AIAA-2008-523*.

Theodorsen, T. [1935] "General theory of aerodynamic instability and the mechanism of flutter," NACA TR 496.

Vezza, M. and Galbraith, R. A. McD. [1985] "A method for predicting unsteady potential flow about an airfoil," *International Journal for Numerical Methods in Fluids*, **5**, 347-356

Visbal, M. R. [1986] "Evaluation of an implicit Navier-Stokes solver for some unsteady separated flows," *AIAA Paper No. AIAA-86-1053*.

Visbal, M. R. and Shang, J. S. [1989] "Investigation of the flow structures around a rapidly pitching airfoil," *AIAA J.*, **27(8)**.

Visbal, M. R. and Gaitonde, D. V. [1999] "High-order-accurate methods for complex unsteady subsonic flows," *AIAA J.*, **37 (10)**, 1231-1239.

Visbal, M. R. and Gaitonde, D. V. [2002] "On the use of high-order finite-difference schemes on curvilinear and deforming meshes," *Journal of Computational Physics*, **181**, 155-185.

Von Kármán, T. and Sears, W. R. [1938] "Airfoil theory for non-uniform motion," *Journal of the Aeronautical Sciences*, **5(10)**, 379-390.

Wilson, J. R. [1998] "Mini technologies for major impact" Aerospace America, May 1998, 36-42.

Wu, T. Y. [1971] "Hydromechanics of swimming of fishes and cetaceans," *Advances in Applied Mechanics*, **11**, 1-63.

Xiao, Q. and Liao, W. [2009] "Numerical study of asymmetric effect on a pitching foil," *Int. J. Modern Physics C*, **20(10)**, 1663-1680.

Young, J. and Lai, J. C. [2004] "Oscillation frequency and amplitude effects on the wake of a plunging airfoil," *AIAA J.*, **42(10)**, 2042-2052.

Yu, M.L., Hu, H., and Wang, Z. J. [2010] "A numerical study of vortex-dominated flow around an oscillating airfoil with high-order spectral difference method," *AIAA Paper No. AIAA 2010-726*.

Zhang, Y., Ye, Z., and Xie, F. [2012] "Computational investigation of a doubly hinged flapping airfoil," *AIAA J.*, **50(12)**, 2643-2654.